Available online at www.sciencedirect.com
ScienceDirect
Trans. Nonferrous Met. Soc. China 29(2019) 2078−2089
Transactions of Nonferrous Metals Society of China
www.tnmsc.cn

Diffusional transformation in Ti6Al4V alloy during isothermal compression

K. MUTOMBO[1], C. SIYASIYA[2], W. E. STUMPF[2]

1. Council for Scientific and Industrial Research (CSIR), Pretoria 0001, South Africa;
2. Department of Materials Science and Metallurgical Engineering, University of Pretoria, Pretoria 0001, South Africa

Received 6 June 2018; accepted 27 August 2019

Abstract: Thermodynamic calculation of the two-phase Ti alloy was completed using CompuTherm Pandat™ and Ti data base, followed by isothermal compression of Ti6Al4V (Grade 5), with an initial colony lamellar structure that was performed in the (α+β) and β-phase field. Microstructural evolution and phase transformation were investigated using X-ray diffraction, scanning and transmission electron microscopy. The presence of the Ti_3Al or α_2 (hcp), the phase stability and transition temperatures were predicted by the Gibbs free energy−temperature and phase fraction−temperature diagrams. The isothermal compression in the (α+β)-phase field is characterized by reorientation and localized kinking of α/β lamellae, and cracking at α/β interphase regions. While in the $\alpha\rightarrow\beta$-phase transformation area, deformation in β-phase and at α/β interphase boundaries, extensive transformation of α into β-phase, martensitic transformation and spheroidization of α-laths mainly characterize this isothermal compression. A complete transformation of α into β single phase occurs in the β-phase field. Ti_3Al or α_2 (hcp), β (bcc) and α (hcp)-phase, and additional hcp α' and orthorhombic α'' phases in a deformed Ti6Al4V are revealed. The flow stress level, the dynamic recovery and dynamic globularization are affected by deformation temperature.

Key words: Ti6Al4V; phase transformation; spheroidization; thermodynamic calculation

1 Introduction

The Ti6Al4V alloy, the most common dual-phase Ti alloy, has high specific strength, good fatigue and corrosion resistance. These properties are strongly affected by the phases present and their microstructural morphology. In addition, this alloy exhibits an allotropic transformation at the β-transus temperature, changing from a bcc (β-phase) to an hcp (α-phase) crystal structure. The $\alpha\rightarrow\beta$ transformation can only take place by a diffusion controlled by a nucleation and growth process; however, β into α-hcp transformation can either occur by a martensitic shear transformation or diffusion controlled by a nucleation and growth process depending on the cooling rate [1]. Both reactions $\alpha\rightarrow\beta$ and $\beta\rightarrow\alpha$ or $\beta\rightarrow\alpha'$, play an important role in, not only controlling the final microstructure and hence, the mechanical properties of the alloy, but also the deformation behavior.

During the diffusional reconstructive transformation of α into β-phase [2,3], the α-phase nucleates and grows from β grain boundaries, conversely the β-phase grows from the pre-existing β-phase before the transformation temperature exceeded the β-transus, and significant β-phase grows subsequently below the β-transus temperature. The growth of the already existing β-phase is thermodynamically more favorable than the nucleation of new β-phase from α matrix [4−6]. The deformation phase field and quenching rate after the hot compression of two-phase alloys affect the rate of β into α-phase transformation and subsequently affect the final phase also [7].

The β into α'-phase reaction, which is a displacive martensitic transformation, is controlled by shear strain, as opposed to relatively small volume changes in a diffusional transformation. This diffusionless martensitic reaction occurs at relatively higher and intermediate cooling rates, which suppresses or slows down the diffusion of alloying elements in favor of the shear displacement of atoms [3,5].

Evidently, a wide range of phases may be generated depending on temperature, stress, plastic strain, strain rate and chemistry of the two-phase Ti alloys [8−11]. Similarly, these parameters extensively affect the deformation behavior, the microstructural behavior and even the spheroidization of α-laths. Compressive stress

Corresponding author: K. MUTOMBO; E-mail: KMutombo@csir.co.za
DOI: 10.1016/S1003-6326(19)65114-9

and plastic strain accelerate the phase transition by several orders of magnitude by reducing the reaction time and creating additional nucleation sites such as kinked α/β lamellae, secondary grain boundaries, deformation bands and dislocations.

The simultaneous occurrence of deformation and diffusion or displace transformation in two-phase Ti alloys such as Ti6Al4V is not profoundly discussed in most of the hot working studies [12−17] of these alloys. This phase transformation during hot deformation might be a very influential process on the plastic flow behavior, the deformation mechanism of the alloy [12,18,19] and its microstructural evolution, and even affect the dynamic globularization (DGB) [16,17,20,21] of α-laths.

Therefore, this study was aimed to determine the occurrence of phase transformations, and accurately specify a temperature range where the concurrent processes such as spheroidization and phase transition might occur during isothermal compression of Ti6Al4V alloy.

2 Experimental

The Ti6Al4V alloy (Grade 5), in the annealed condition, was supplied by BAOTI Titanium Industry as a billet of 65 mm in diameter and 2540 mm in length. The chemical composition of this alloy is given in Table 1.

Table 1 Chemical composition of Ti6Al4V alloy (Grade 5) (wt.%)

Al	V	O	Fe	C
6.35	4.210	0.185	0.035	0.015
N	Y	H	Others	Ti
0.015	<0.005	0.003	<0.400	Bal.

In order to predict the stability and transition of existing phases in Ti6Al4V during hot compression, thermodynamic calculations were completed using the CompuTherm Pandat™ [22] software and their Ti data base. Ti−Al and Ti−Al−V phase diagrams and the transition of α and β-phase and their thermodynamic stability from room-temperature (RT) to 1200 °C, under equilibrium conditions, were predicted to investigate the effect of temperature on the transformation of existing phases. The phase formation and Gibbs energy phase stability diagrams were superimposed to investigate the effect of deformation temperature, phase content, and the difference in the Gibbs free energy on the microstructural evolution during hot compression.

The hot compression tests were performed in a Gleeble™ 1500D thermo-mechanical simulator. Cylindrical Ti6Al4V samples were wire cut and machined to 10 mm in diameter and 15 mm in height, as shown in Fig. 1(a). Isothermal compression tests were carried out in the temperature range of 650−1100 °C, at a strain rate of 0.01 s^{-1} and to the strain of 0.9. The hot compression schedule is shown in Fig. 2. Two tungsten carbide (WC) anvils and Ta foils, with silica glass barriers around these anvils, were used to minimize the temperature gradient along the length of the sample (Fig. 1(b)). A friction coefficient of 0.3, between the Ti6Al4V sample and Ta foil, was assumed. The von Mises flow stress was calculated from the expression given by DIETER [23]. From these corrected flow stress curves, the steady state flow stress (σ_{ss}) and the peak strain (ε_p) were read off and the mean flow stress (MFS) was estimated.

In order to investigate the microstructural evolution and phase present in the deformed Ti6Al4V, samples were prepared according to the requirements of ASTM standard E3-01. The compressed specimens were cut parallel to their compression direction (Fig. 1(c)), mechanically ground, and polished etched using Keller's reagent according to the ASTM standard E340-00.

The metallographic observation was performed using light optical microscopy (LOM) and Jeol™ scanning electron microscopy (SEM) equipped with energy dispersive X-ray spectroscopy (EDX).

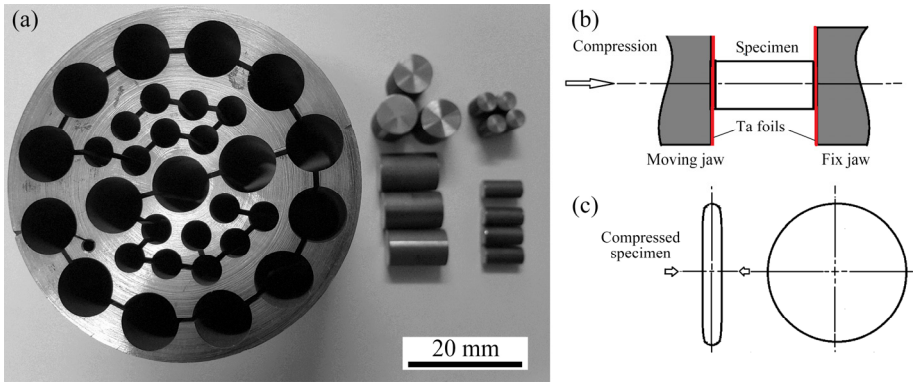

Fig. 1 Wire-cut and machined compression specimens (a), and schematics of shape of specimen before (b) and after (c) compression

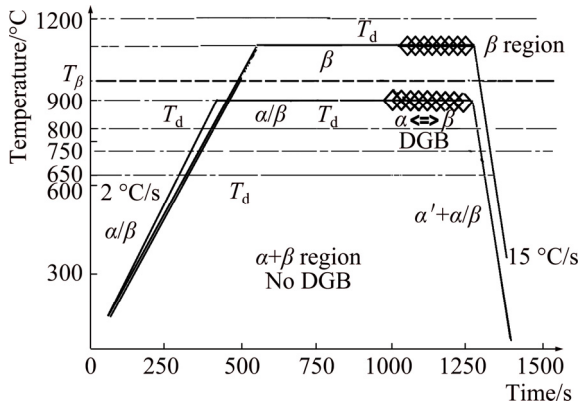

Fig. 2 Schematic of hot compression cycle of Ti6Al4V with colony lamellar, in (α+β) and β-phase field (heating rate 2 °C/s, cooling rate 15 °C/s, T_d−deformation temperature)

Ti6Al4V samples, in the deformed conditions, were cut to about 3 mm in thickness and 15 mm in diameter, ground, polished and etched to reveal the area of interest during ion milling. The cutting and thinning of transmission electron microscopy (TEM) specimens were performed with Zeiss™ focused ion beam and scanning electron microscope (FIB-SEM).

The high resolution TEM (HR-TEM) Tecnai™ G2 F20 X-Twin MAT with field emission gun was utilized to identify existing phases and investigate the microstructural change during and after the hot compression.

X-ray diffraction (XRD) analysis was done on the compressed samples to investigate the phase transition in Ti6Al4V during the hot compression. The samples were analyzed using a Panalytical X'Pert Pro powder diffractometer in θ−θ configuration with an X'Celerator detector, variable divergence and fixed receiving slits with Fe filtered Co K_α radiation (λ=1.789 Å). Phases were identified using X'Pert Highscore plus software.

3 Thermodynamic and experimental results

The diagrams of formation and stability of phase in an equilibrium condition in Ti6Al4V, and phase diagrams of Ti−Al−V and Ti−Al systems, calculated using Pandat™, are presented in Fig. 3.

The existence of β-phase (bcc), α_2-phase Ti_3Al (hcp) and α-phase (hcp) is revealed by the phase formation diagram (Fig. 3(a)). These three phases coexisted from room temperature (RT) to about 625 °C. However, only α and β-phases were present in the temperature range of 625−960 °C. The α_2-phase completely transformed to α-phase when the temperature reached 625 °C (Fig. 3(a)). The Ti6Al4V consisted only of β single phase above the β-transus temperature of 960 °C. In the temperature range from 25 to about 720 °C, the α-phase had the lowest Gibbs free energy (ΔG_α<$\Delta G_{\alpha 2}$<ΔG_β), while in the temperature range from 720 to about 850 °C, the Gibbs free energy of α-phase was lower than that of the β-phase (ΔG_α<ΔG_β). However, the Gibbs free energy of the β-phase is the lowest above 890 °C, i.e., the β-phase became the most stable phase above 890 °C, as shown by

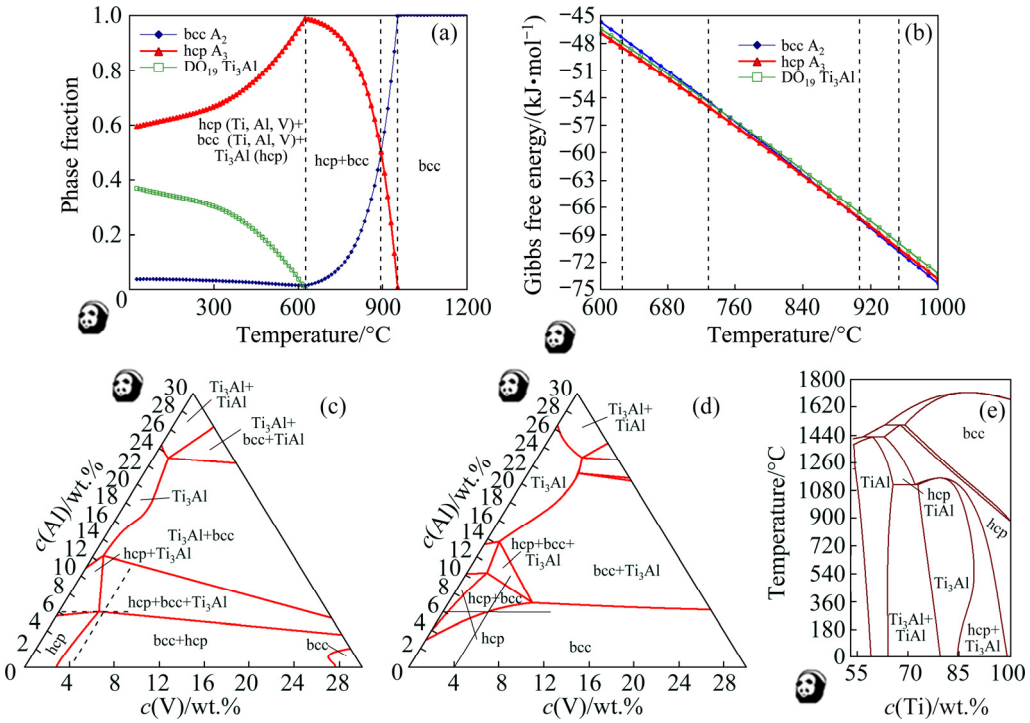

Fig. 3 Diagrams of phase formation (a), phase stability of Ti6Al4V in equilibrium condition (b), Ti−Al−V at 624.14 °C (c), Ti−Al−V at 953.73 °C (d) and Ti−Al systems (e), calculated using Pandat™ Software

the phase stability diagram (Fig. 3(b)). The point of equal Gibbs free energy of −6450 J/mol ($\Delta G_\alpha=\Delta G_\beta$), was reached in the temperature range from about 860 to 890 °C.

The Ti-rich corners of the Ti−Al−V ternary phase diagrams, as calculated at 624 and 953.73 °C, are shown in Fig. 3(c) and Fig. 3(d), respectively. At 624 °C, an eutectoid reaction (bcc+hcp→hcp+bcc+Ti_3Al) occurred at the alloy composition of 90 wt.% Ti, 6 wt.% Al and 4 wt.% V as for Ti6Al4V. The minimum amount of Al needed to precipitate the intermetallic Ti_3Al as a pure compound and as a mixture of ($\alpha+\alpha_2$) is shown in Fig. 3(e).

The reactions, $\alpha\rightarrow\alpha_2$ (ending at about 625 °C) and $\alpha\rightarrow\beta$ (ending at about 960 °C) are revealed by the phase stability diagram (Fig. 3(a)) as well. The absolute value of the Gibbs free energy (ΔG) decreases with increasing the temperature. The α-phase is the most stable phase in the temperature range from RT to 850 °C ($|\Delta G_\alpha|>|\Delta G_\beta|$ and $|\Delta G_\alpha|>|\Delta G_{\alpha_2}|$). In the temperature from about 860 to 890 °C, the β-phase becomes as thermodynamically stable as the α-phase ($|\Delta G_\alpha|=|\Delta G_\beta|$). Above 890 °C, the most stable phase is the β-phase ($|\Delta G_\beta|>|\Delta G_\alpha|>|\Delta G_{\alpha_2}|$). The minimum content of Al needed to precipitate the intermetallic Ti_3Al as a mixture ($\alpha_2+\alpha$) is about 4 wt.%.

The Ti64Al4V alloy may contain different phases such as α, α_2, β, α' and α'' depending on the prior thermal treatment performed. These phases transform at specific temperatures which can be determined by the thermodynamic measurements.

The superimposed phase formation and phase stability diagram is shown in Fig. 4. According to the specific temperature of phase transition in each case, three different regions are observed:

(1) The ($\alpha+\beta$)-phase region, in which the $\alpha\rightarrow\beta$ phase transformation is thermodynamically unfavorable.

(2) The ($\alpha\rightarrow\beta$)-phase transformation field, in which the reversible $\alpha\leftrightarrow\beta$ phase transformation is thermodynamically unfavorable in the temperature range from 760 to about 850 °C, however, this reaction ($\alpha\leftrightarrow\beta$) becomes favorable in the temperature range from 850 to about 890 °C; and the complete $\alpha\rightarrow\beta$ phase transformation becomes thermodynamically favorable in the temperature range from 890 to about 960 °C.

(3) The β-phase region, in which one single β-phase exists.

The flow stress curves of the Ti6Al4V, with a colony lamellar starting microstructure, isothermally deformed to the strain of 0.9, at a strain rate of 0.01 s^{-1} and in the temperature range of 650−1100 °C, are shown in Fig. 5.

At a strain rate of 0.01 s^{-1} and at temperatures of 650 and 750 °C, the flow stress curve exhibits strain hardening up to a peak stress (σ_p), followed by a continuous softening without reaching a steady state stress. In the temperature range of 800−950 °C, the strain hardening is followed by a gradual softening with increasing plastic strain before reaching a steady state stress (DRX). Strain hardening is followed directly by a steady state stress (DRV) above the β-transus or in the temperature range of 1000−1100 °C.

The initial starting microstructure of the Ti6Al4V alloy is shown in Fig. 6. Colonies and α/β lamellae

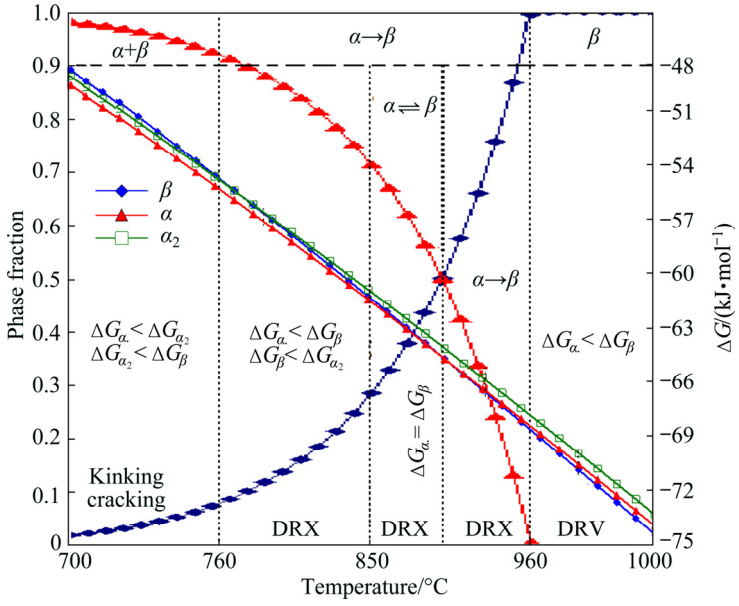

Fig. 4 Schematically superimposed diagram combining phase formation and phase stability (Gibbs energy) diagrams under equilibrium conditions (Phase transition temperatures are shifted by some degrees under effect of strain rate and strain which introduce non-equilibrium conditions)

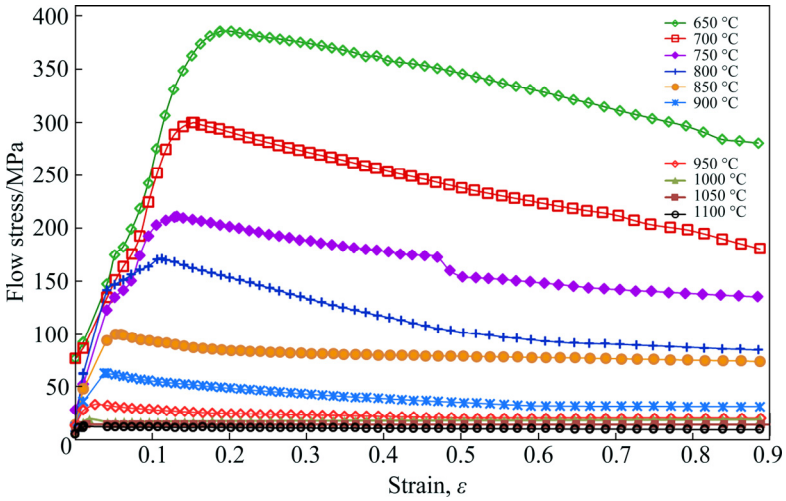

Fig. 5 Isothermal compression curves at 0.01 s^{-1} and in temperature range of 650−1100 °C of Ti6Al4V with colony lamellar initial starting structure

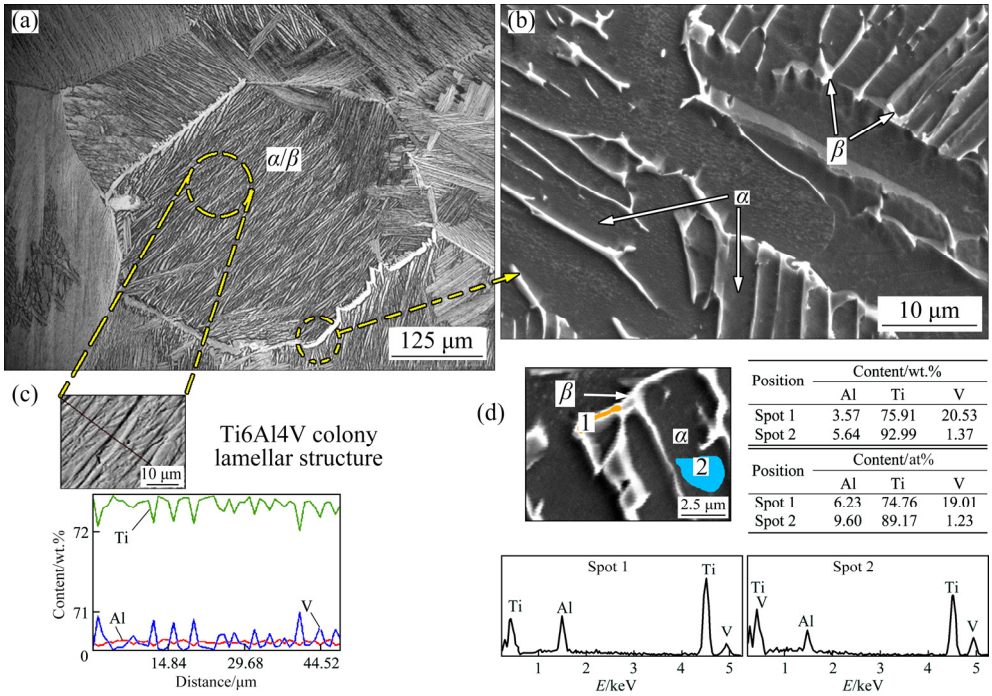

Fig. 6 Initial starting microstructure of Ti6Al4V: (a) Colonies and α/β lamellae; (b) Morphology of α and β-phase; (c) Distribution of Al and V in Ti; (d) V, Al and Ti content in α and β-phase

(Fig. 6(a)), and the partition of Al and V in Ti (Fig. 6(c)) are revealed. The morphology and V, Al and Ti contents in α and β-phase are shown in Figs. 6(b) and (d), respectively.

The macroscopic observations of the isothermally compressed Ti6Al4V at 1000 °C (in β-phase field) and at 800 °C (in $\alpha\rightarrow\beta$-phase field) are shown in Figs. 7(a) and 7(b), respectively. This observation reveals a homogenously distributed and elongated primary β-grains in Ti6Al4V compressed in the β-phase region (above the β-transus), as shown in Fig. 7(a). However, the heterogeneous structure is observed in Ti6Al4V deformed in the ($\alpha\rightarrow\beta$)-phase region. Three distinct zones are revealed in Ti6Al4V isothermally compressed in the ($\alpha\rightarrow\beta$)-phase region (800 °C): the zone of little deformation (LDZ) or the zone of almost no deformation (NDZ), the zone of moderate deformation (MDZ) and the zone of intense shearing (ISZ) (Fig. 7(b)) [20]. In the LDZ or NDZ, the reorientation, kinking and cracking of α/β lamellae are not observed; however, in the MDZ, a partial reorientation, kinking and cracking of α/β lamellae may occur. A complete reorientation of α/β lamellae is observed in ISZ.

The resulting microstructures of Ti6Al4V with an

initial starting lamellar structure deformed at a strain rate of 0.01 s^{-1} and at deformation temperature of 650 °C (in $\alpha+\beta$ field) and 750 °C (in $\alpha+\beta$ field), are shown in Figs. 8(a) and (b), respectively. At 650 °C, the α-laths remain almost unchanged besides some localized kinking. However, the cracking in the α-GBs/β-phase interphase boundaries (Fig. 8(c)) is prevalent below 750 °C. At the compression temperature of 750 °C, most of the α-laths

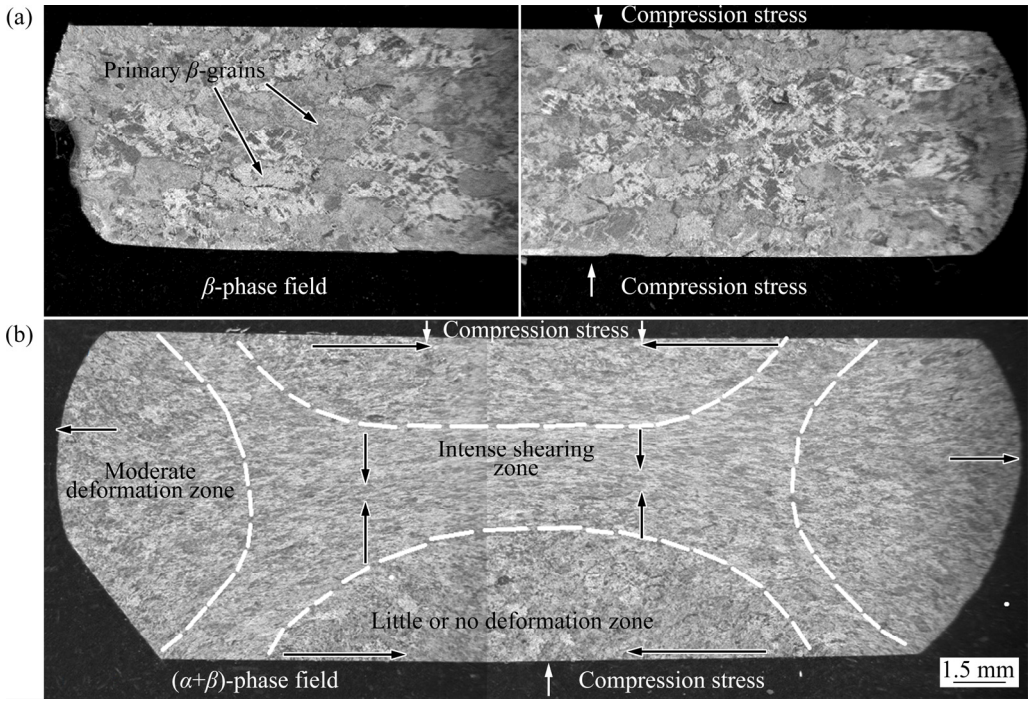

Fig. 7 Macroscopic observations of isothermally compressed Ti6Al4V at 1000 °C: (a) Homogenous deformation zone with elongated grains; (b) Flow localization zones showing little deformation zone (LDZ) or almost no deformation zone (NDZ), moderate deformation zone (MDZ) and intense shearing zone (ISZ)

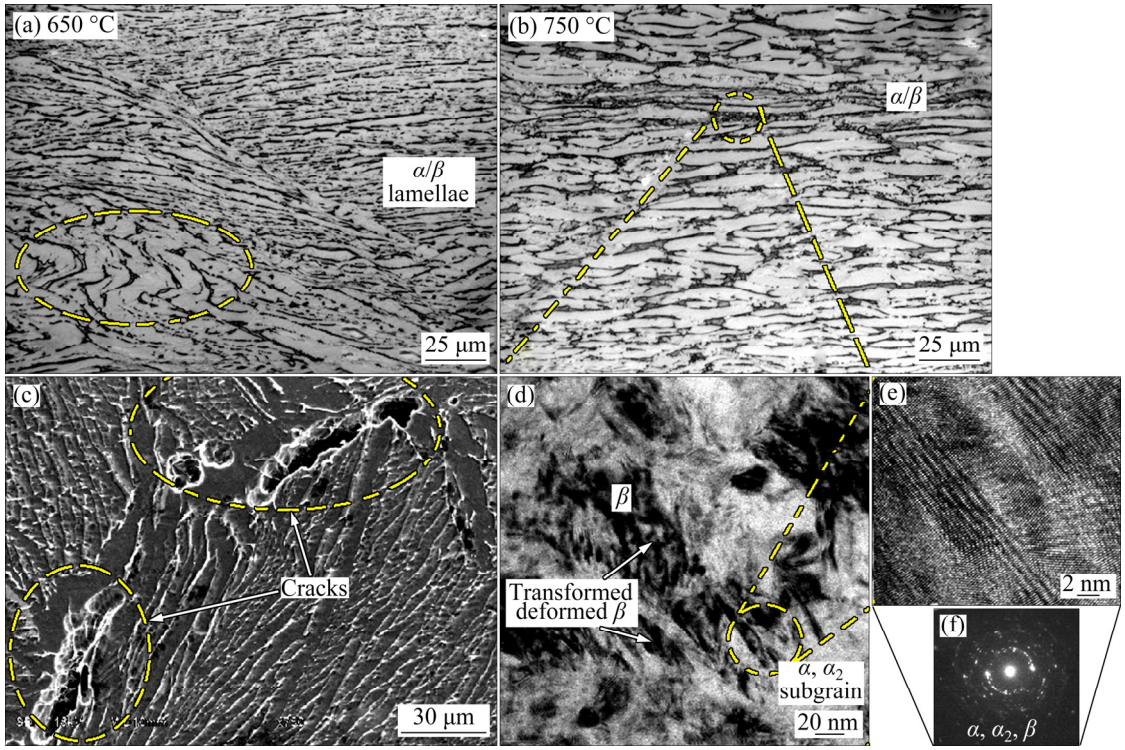

Fig. 8 Resulting microstructures of Ti6Al4V with initial lamellar structure deformed at strain rate of 0.01 s^{-1} and at deformation temperature of 650 and 750 °C (in $\alpha+\beta$ phase field): (a, b) α-laths and kinked α-laths; (c) Cracks; (d) Deformed β and α/β interphase; (e) HR-TEM image; (f) Phases

are reoriented perpendicularly to the compression stress (Fig. 7). Deformed areas are observed in the β-phase and at α/β interphase boundaries, as shown in the TEM image (Fig. 8(d)), and HR-TEM and diffraction pattern images (Figs. 8(d) and (e), respectively).

The resulting microstructures of Ti6Al4V deformed at a strain rate of 0.01 s^{-1} and at deformation temperature of 850 °C (in $\alpha\rightarrow\beta$ transformation field) and 900 °C (in $\alpha\rightarrow\beta$ transformation field), are shown in Figs. 9(a) and 9(b), respectively. Most of the α-laths are spheroidized at these deformation temperatures. Slight transformation of α into β-phase which leads to α' martensitic structure and β-phase on the grain boundaries upon cooling is observed in Figs. 9(c) and (d).

The resultant microstructures of Ti6Al4V alloy compressed at a strain rate of 0.01 s^{-1} and at the deformation temperatures of 950 °C (very close to β-transus temperature) and 1050 °C (in β-phase field), are respectively shown in Figs. 10(a) and (b). Elongated primary β-grains with α-globules on grain boundaries, and a partial martensitic structure within the grains are revealed in Fig. 10(a). However, coarser primary β-grains and a partial martensitic structure are observed in Fig. 10(b). The martensitic structure might result from extensive transformation of α into β-phase, which leads to a considerable amount of retained β, α' martensite upon cooling (Figs. 10(c) and (d)).

The crystal diffraction patterns of the Ti6Al4V deformed at a strain rate of 0.01 s^{-1} and deformation temperatures of 800 °C (in $\alpha\rightarrow\beta$ transformation field), are shown in Fig. 11. The deformed β grains, $\alpha+\beta$ and α/β interphase areas are revealed in Figs. 11(a), (b) and (c). The α-phase deformed in the ($\alpha+\beta$) area and the ($\alpha/\beta+\alpha'$) structure are revealed in Figs. 11(b) and (c). The α/β deformed interphase and dislocation lines are more visible in Fig. 11(c). The HR-TEM image, in Fig. 11(d), reveals the structure of the α/β deformed interphase constituent. The crystal structures of α_2-hcp, α-hcp, and β-bcc are revealed by SAEDs in Figs. 11(e), (f) and (g), respectively.

The additional crystal diffraction patterns of the deformed areas of Ti6Al4V compressed at a strain rate of 0.01 s^{-1} and at deformation temperature of 950 °C (very close to β-transus temperature) and 1050 °C (in β-phase field), are shown in Fig. 12. The α/α, and α/β interphase constituents, and the ($\alpha+\alpha_2$) structure are revealed in Figs. 12(a) and (b), respectively. The HR-TEM images (Figs. 12(c) and (e)) reveal the dissimilarity between the α-phase and ($\alpha+\alpha_2$) structures. The crystal diffraction patterns of α-hcp and α_2-hcp are shown on SAEDs in Figs. 12(d) and (f), respectively.

The presence of different phases α, α_2 and β, in Ti6Al4V isothermally compressed at 0.01 s^{-1} and in the deformation temperature range of 650−1000 °C, is revealed by X-ray diffraction in Fig. 13. The Ti6Al4V compressed at 650 °C (in $\alpha+\beta$ field) and 700 °C (in $\alpha+\beta$

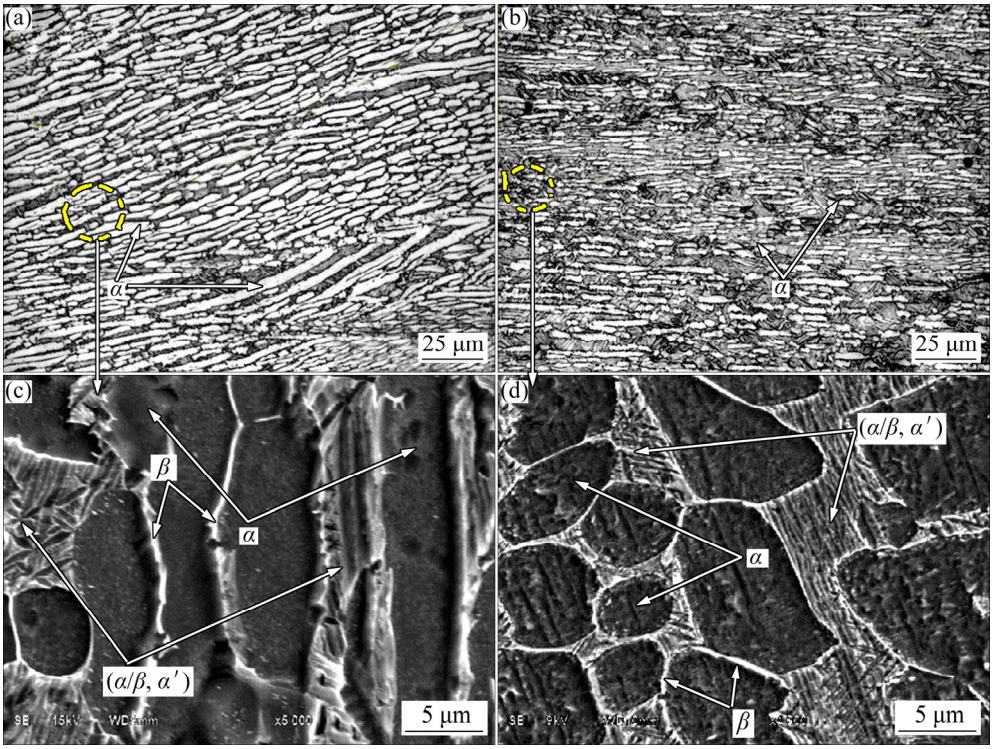

Fig. 9 Resulting microstructures of Ti6Al4V deformed at strain rate of 0.01 s^{-1} and at deformation temperatures of 850 °C (in $\alpha\rightarrow\beta$ transformation field) (a) and 900 °C (in $\alpha\rightarrow\beta$ transformation field) (b), and SEM images showing partial martensitic structure (α/β, α'), β-boundaries and α-globules (c, d)

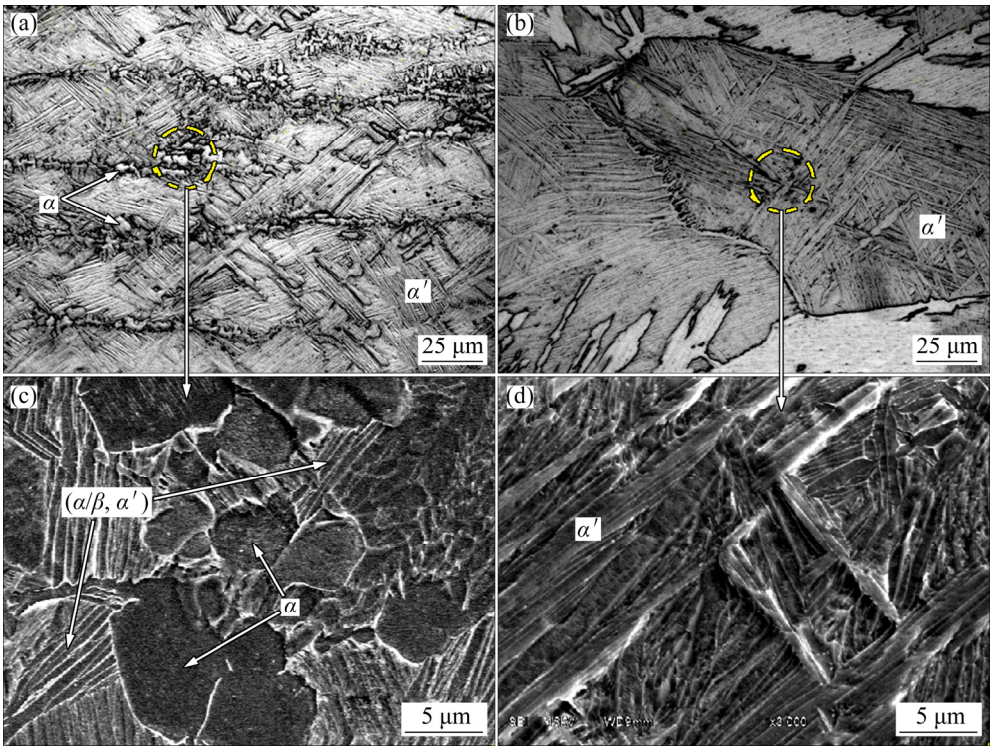

Fig. 10 Resultant microstructures of Ti6Al4V deformed at strain rate of 0.01 s^{-1} and deformation temperatures of 950 °C (very close to β-transus temperature) (a, c) and 1050 °C (in β-phase field) (b, d): (a) Primary β-grains; (b, d) Martensitic α' structure; (c) Spheroidized α-phase on grains

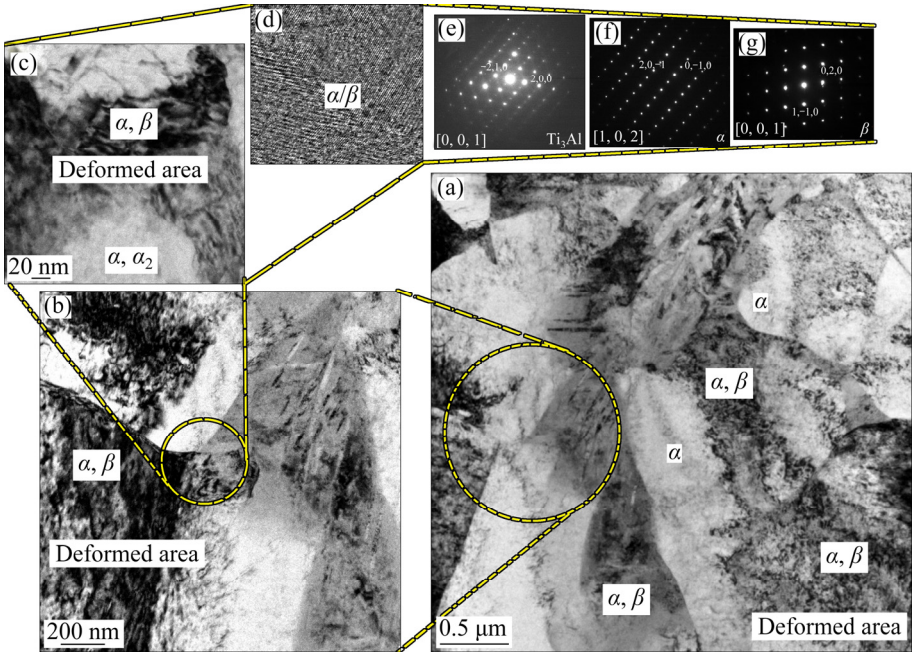

Fig. 11 Crystal diffraction patterns of Ti6Al4V deformed at strain rate of 0.01 s^{-1} and deformation temperatures of 800 °C (in $\alpha \rightarrow \beta$ transformation field): (a, b) Deformed β grains, (α+β) and α, β and α' needles at α/β interphase areas; (c) Deformed α/β interphase and dislocations; (d) HR-TEM image of structure of deformed α/β interphase; (e) SAED of α_2 (hcp); (f) SAED of α (hcp); (g) SAED of β (bcc)

field) shows a colony lamellar structure morphology and mostly contains α (hcp), α_2 (hcp), β (bcc). However, the Ti6Al4V compressed at 850 °C (in $\alpha \rightarrow \beta$ transformation field), and 1000 °C (in β-phase field) shows a martensitic structure morphology containing additional phases of α' (hcp) and α'' (orthorhombic).

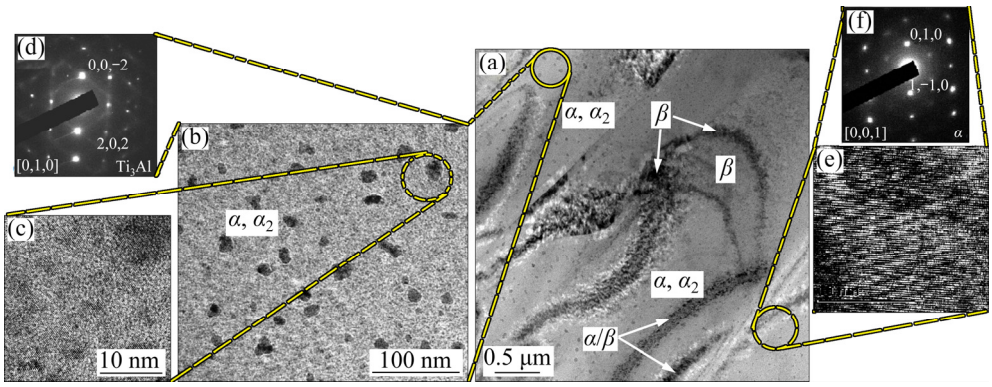

Fig. 12 $\alpha+\alpha_2$ crystal diffraction patterns of deformed areas of Ti6Al4V compressed at strain rate of 0.01 s^{-1} and at deformation temperature of 1050 °C: (a) α/β interphases, β-phase and ($\alpha+\alpha_2$) structure; (b) ($\alpha+\alpha_2$) structure; (c) HR-TEM image of ($\alpha+\alpha_2$)-phase; (d) SAED image of α_2-hcp crystal; (e) HR-TEM image of α-phase structure; (f) SAED image of α-hcp crystal

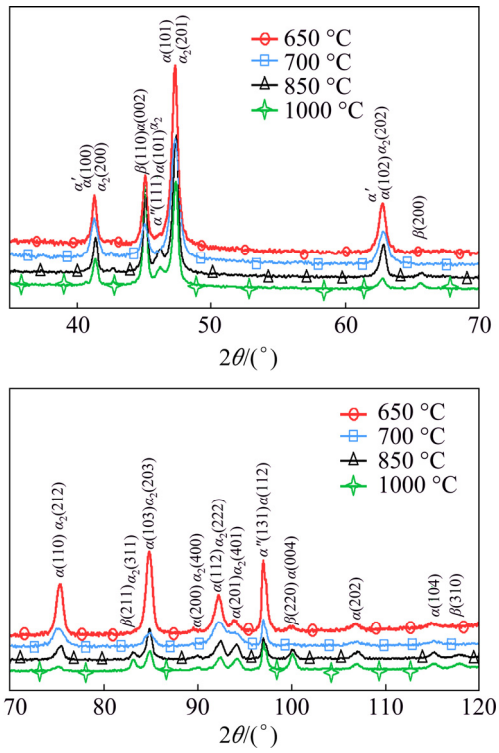

Fig. 13 X-ray diffraction patterns of Ti6Al4V isothermally compressed at strain rate of 0.01 s^{-1} and at deformation temperatures of 650 °C (in $\alpha+\beta$ field), 700 °C (in $\alpha+\beta$ field), 850 °C (in $\alpha\rightarrow\beta$ transformation field), and 1000 °C (in β-phase field)

4 Discussion

The thermodynamic calculation reveals the existence of the α-phase (hcp), bcc phase (β) and Ti_3Al phase (α_2) below 625 °C (Fig. 3(a)). The Ti_3Al is an ordered hcp superlattice (DO_{19}) and an intermetallic compound which is unlike the disordered α-phase (hcp) structure [2]. In the temperature range of 625−960 °C, only α and β phases exist. Above 625 °C, the Ti_3Al phase entirely disappears. The Ti6Al4V becomes a single β-phase alloy above 960 °C.

Below 760 °C, the α-phase possesses the lowest Gibbs free energy followed by the α_2-phase; however, the β-phase starts to become stable above 960 °C (Fig. 3(b)). The region of equal Gibbs free energy (of about −6450 J/mol) for α and β-phase exists in the temperature range from about 860 to 890 °C (where $\alpha \rightleftharpoons \beta$ reversible reaction is spontaneous). At this specific point, the two phases, α and β, are not at full equilibrium but have a specific (Al+V) content, as illustrated in Fig. 14.

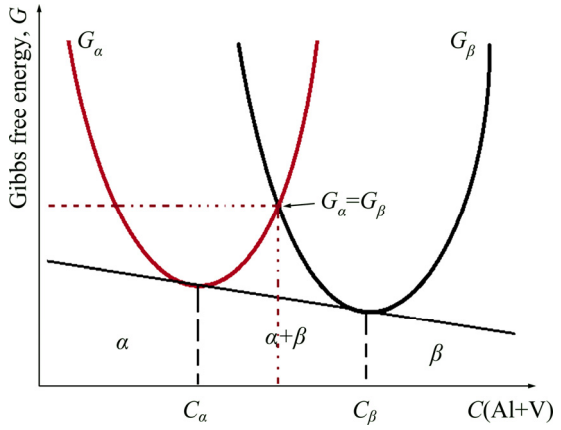

Fig. 14 Schematic illustration of variation of Gibbs free energy (G) as function of α and β-phase content C in Ti−Al−V alloy at specific temperature

The transformation of α into β ($\alpha\rightarrow\beta$) is thermodynamically possible above 625 °C and becomes more spontaneous above 700 °C due to an increase in temperature and the Gibbs free energy of β ($|\Delta G_\beta|$). In addition, the kinetics of the $\alpha\rightarrow\beta$ reaction increases as the temperature and the diffusion rate of elements increase.

An eutectoid reaction (bcc+hcp→hcp+bcc+Ti_3Al) indicates the reactions $\alpha\rightarrow\beta$, $\beta\rightarrow\alpha$ and $\alpha\rightarrow\alpha_2$ at the alloy composition of 90 wt.% Ti, 6 wt.% Al and 4 wt.% V on the Ti−Al−V ternary phase diagrams (Fig. 3(c)). The phase fraction of β (bcc) remains unchanged up to 625 °C; however, that of Ti_3Al decreases as the phase fraction of α (hcp) increases (Fig. 3(a)). Evidently, the Ti_3Al (ordered hcp structure) transforms to α-phase (disordered hexagonal phase) during heating. Therefore, the overall reaction at this point can be expressed as

$$\alpha+\beta+\alpha_2\rightarrow\alpha+\beta \text{ or } \alpha_2\rightarrow\alpha \quad (1)$$

The eutectoid reaction at about 954 °C (bcc→hcp+bcc) on the ternary phase diagram (Fig. 3(d)) corresponds exactly with the transition point at about 960 °C (Fig. 3(a)) where the α-phase completely transforms in β-phase according to the reaction below:

$$\alpha+\beta\rightarrow\beta \quad (2)$$

Accordingly, the phase transformation sequence on cooling from the β-phase can be given as

$$\beta\rightarrow\alpha+\beta\rightarrow\alpha+\beta+Ti_3Al \quad (3)$$

The existence of the Ti_3Al has also been reported in high Al content Ti alloys such as Ti40Al10V, by SHAO et al [24]. However, the effect of fine α_2 particles on mechanical properties and, quasi-static and dynamic torsional properties in Ti6Al4V alloy has been discussed by CARREON et al [25] and LEE et al [26]. This order−disorder transformation depends on the chemical composition of the alloy and the transformation temperature. At about 600 °C, the affinity of Ti and Al atoms to localize particular positions in the lattice overcomes the unsystematic action of thermal agitation and leads to an ordered Ti_3Al structure [2].

The α-phase is the most stable phase in the (α+β)-phase region, i.e. below 625 °C and the reversible reaction of α into β or β into α is possible above 700 °C in the ($\alpha\rightarrow\beta$)-phase transformation field ($|\Delta G_\alpha|>|\Delta G_\beta|>|\Delta G_{\alpha_2}|$) (Fig. 4). However, the β-phase is the most thermodynamically stable phase above 890 °C, i.e., in ($\alpha\rightarrow\beta$)-phase transformation region and in the β-phase field as $|\Delta G_\beta|>|\Delta G_\alpha|>|\Delta G_{\alpha_2}|$.

The presence of α, α_2 and β-phase is evidently confirmed by the X-ray diffraction analysis (Fig. 13) in the isothermally deformed Ti6Al4V at strain rate of 0.01 s^{-1} and in the deformation temperature range of 650−1000 °C. Additionally, the orthorhombic martensite (α'') and hexagonal martensite (α') are revealed in Ti6Al4V compressed at 850 and 1000 °C. Furthermore, α''-martensite transforms at lower temperatures compared to α'-martensite [27]. The transition temperatures of these non-equilibrium reactions $\beta\rightarrow\alpha'$ (at about 1000 °C) and $\beta\rightarrow\alpha''$ (at about 600 °C) have been determined using the dilatometry method [1].

The transformation of β-phase into orthorhombic α''-martensite ($\beta\rightarrow\alpha''$) is possible at 600 °C in non-equilibrium conditions, i.e., during the quenching of β-phase [1]. The reactions $\alpha\rightarrow\alpha_2$ (at 625 °C) and $\alpha\rightarrow\beta$ (at 960 °C) are thermodynamically possible in the (α+β)-phase and ($\alpha\rightarrow\beta$) phase transformation fields, while the transformation of β-phase into α'-martensite ($\beta\rightarrow\alpha'$) [1] is possible in non-equilibrium conditions, i.e., during the quenching of β-phase from ($\alpha\rightarrow\beta$) phase transformation or β-phase field to (α+β)-phase region (Fig. 4).

The isothermal compression of Ti6Al4V with an initial colony lamellar structure in the (α+β) field is controlled by the reorientation of lamellae (in ISZ) in the direction perpendicular to the compressive stress (Fig. 7(b)), localized kinking (in MDZ) of α/β lamellae and cracking at α/β interphase regions (Figs. 8(a) and (c)). The kinked and cracked regions, especially in the β-phase and α/β interphases are highly-strained areas (TEM image in Fig. 11), which could be due to prism or only ⟨c+a⟩ pyramidal slip systems of the hcp crystal structure operating in these isolated regions (shear band or flow localization) [28,29]. The grain and phase boundary deformation sliding during the isothermal compression of Ti6Al4V in the (α+β) field may be mainly due to shear stresses. Obviously, the cracking, fragmentation or breakup of the β-phase and α/β interphase is basically caused by the shear stresses in the ISZ.

The heterogeneous deformation is characteristic of isothermal compression in the ($\alpha\rightarrow\beta$)-phase region. The kinking of α-laths in moderate deformation zone and their complete reorientation in intense shear zone are attributed to tension and shear stresses, respectively (schematically shown in Fig. 7). However, the transformation of α into β-phase leading to the formation of α'', α' and β-phase after quenching is firstly the result of α into β reaction in ($\alpha\rightarrow\beta$) field which is induced by large plastic strain, and secondly the transformation of β into α' and α''-martensite during quenching. The free energy reduction caused by a free Gibbs energy decrease ($|\Delta G_\beta|>|\Delta G_\alpha|$) may be the driving force for this simultaneous deformation−transformation process.

The temperature dependence of the flow stress (σ) is hence driven by the change of phase fraction (α/β-phase) and thermal activation energy in each phase as predicted by the thermodynamic calculations (Fig. 3).

Deformation in β-phase and α/β interphase boundaries, extensive transformation of α into β-phase and spheroidization of α-laths are main characteristics of isothermal compression in the ($\alpha\rightarrow\beta$)-phase field. Reoriented α-laths transform extensively into β-phase, which leads to a considerable amount of retained β, α' and spheroidized α-grains after quenching (Fig. 9). The increase in deformation temperature favors the ($\alpha\rightarrow\beta$)

reaction by increasing the absolute value of the free Gibbs energy of the β-phase ($|\Delta G_\beta|$). The low strain rate and large plastic strain are favorable to the ($\alpha\rightarrow\beta$) reaction as they respectively increase the diffusion time and the nucleation sites. Obviously, the α-phase transforms (α into β-phase transformation) and grows from the β-phase when cooling from β-phase field, while β-phase transforms from α-phase but nucleates and grows from retained β-phase when heating from (α+β) phase field. This is consistent with highly-strained areas observed in β-grains and α/β interphase regions (TEM image in Fig. 11). The dislocation density in the deformed β-phase may be increased by a large plastic strain. This presence of excess dislocations might lead to heterogeneous nucleation of the β-phase provided by the ($\alpha_\varepsilon\rightarrow\beta'_\varepsilon$) transformation. This phase transformation may be retarded due to the substantial reduction of dislocations during dynamic recrystallization. This is consistent with the observation made by HE et al [30] on the occurrence of DRX on deformed grains.

Therefore, the increase amount of retained β (bcc) and especially α' (hcp), and the existence of α'' orthorhombic martensite (X-ray diffraction spectrum in Fig. 13) in Ti6Al4V matrix, is an indication of the strain-inducing ($\alpha_\varepsilon\rightarrow\beta_\varepsilon$) and subsequent ($\beta\rightarrow\alpha'$)-phase after quenching. The β-phase fraction which increases during the isothermal compression in this phase field suggests the enhancement of the kinetics of the ($\alpha\rightarrow\beta$)-phase.

In the temperature range from about 850 to 950 °C, the β-phase becomes more stable than the α-phase as ($|\Delta G_\beta|\geq|\Delta G_\alpha|$) (Fig. 3 or 4). The driving force for the ($\beta\rightarrow\alpha$) transformation in these specific conditions of strain and deformation comes from the Gibbs free energy difference between the α-phase and the β-phase.

A complete transformation of α into β single phase which results in martensitic structure after quenching occurs in the β-phase field. A further increase in the deformation temperature above the β-transus leads initially to the $\alpha\rightarrow\beta$ reaction as ($|\Delta G_\beta|>|\Delta G_\alpha|$), which subsequently suppresses the α-lath globularization. The final structure consists of β-transformed grains containing α, β, α', α'' and α_2 at room temperature. The retained β-phase and α/β interphase boundaries are the most strained areas as well (TEM image in Fig. 11). The homogenous deformation with elongated β-grains (Fig. 7) occurs in this β-phase region.

5 Conclusions

(1) The hcp Ti_3Al (α_2), bcc (β) and hcp (α) phases are revealed in the Ti6Al4V isothermally compressed below 750 °C; however, additional hcp (α') and orthorhombic (α'') phases are found in Ti6Al4V compressed in the temperature range of 750−1100 °C.

(2) Three different regions are observed according to the specific temperature of phase transition: the (α+β)-phase, $\alpha\rightarrow\beta$ phase transformation and β-phase region.

(3) A complete transformation of α into β single phase which results in a martensitic structure after quenching is found in the β-phase field.

(4) Decreasing the deformation temperature slows down the rate of the $\alpha\rightarrow\beta$ phase transition due to a higher Gibbs free energy ($|\Delta G_\alpha|$) which retards the dynamic globularization of α-laths.

(5) Increasing the temperature further above the β-transus temperature, decreases the flow stress level, promotes dynamic recovery and favors the $\alpha\rightarrow\beta$ reaction, which completely suppresses the dynamic globularization of α-laths.

Acknowledgments

The funding of this project by the South African Department of Science and Technology (DST) along with the technical support of the Council for Scientific and Industrial Research (CSIR) and the University of Pretoria are acknowledged.

References

[1] PEI C, FAN Q, CAI H, LI J. High temperature deformation behavior of the TC6 titanium alloy under the uniform DC electric field [J]. Journal of Alloys and Compounds, 2010, 489: 401−407.

[2] MUTOMBO K, SIYASIYA C, STUMPF W. Phase transformation cycle $\beta\rightarrow\alpha'+\alpha+\alpha''\rightarrow\beta$ in Ti6Al4V Alloy [J]. Materials Science Forum, 2015, 828−829: 232−238.

[3] DĄBROWSKI R. The kinetics of phase transformations during continuous cooling of the Ti6Al4V alloy from the single-phase β range [J]. Archives of Metallurgy and Materials, 2011, 56: 6−10.

[4] OBASI G C, MOAT R J, LEO PRAKASH D G, KOCKELMANN W, da QUINTA FONSECA J, PREUSS M. In situ neutron diffraction study of texture evolution and variant selection during the $\alpha\rightarrow\beta\rightarrow\alpha$ phase transformation in Ti−6Al−4V [J]. Acta Materialia, 2012, 60: 7169−7182.

[5] ZHANG M X, KELLY P M. Crystallographic features of phase transformations in solids [J]. Progress in Materials Science, 2009, 54: 1101−1170.

[6] LONARDELLI I, GEY N, WENK H R R, HUMBERT M, VOGEL S C C, LUTTEROTTI L. In situ observation of texture evolution during $\alpha\rightarrow\beta$ and $\beta\rightarrow\alpha$ phase transformations in titanium alloys investigated by neutron diffraction [J]. Acta Materialia, 2007, 55: 5718−5727.

[7] ELMER J W W, PALMER T A A, BABU S S S, SPECHT E D D. In situ observations of lattice expansion and transformation rates of α and β phases in Ti−6Al−4V [J]. Materials Science and Engineering A, 2005, 391: 104−113.

[8] COLLINGS E W. The physical metallurgy of titanium alloys [M]. USA: American Society for Metals, 1984.

[9] SEMIATIN S L. Metalworking: Bulk forming [C]//ASM International 2005. ASM Handbook, Volume 14A , 2005: 552−699.

[10] ZENG L, BIELER T R. Effects of working, heat treatment, and aging on microstructural evolution and crystallographic texture of α, α', α''

and β phases in Ti−6Al−4V wire [J]. Materials Science and Engineering A, 2005, 392: 403−414.
[11] MANSHADI DEHGHAN A, DIPPENAAR R J. Strain-induced phase transformation during thermo-mechanical processing of titanium alloys [J]. Materials Science and Engineering A, 2012, 552: 451−456.
[12] SONG H W, ZHANG S H, CHENG M. Dynamic globularization kinetics during hot working of a two phase titanium alloy with a colony alpha microstructure [J]. Journal of Alloys and Compounds, 2009, 480: 922−927.
[13] SONG H., ZHANG S, CHENG M. Dynamic globularization prediction during cogging process of large size TC11 titanium alloy billet with lamellar structure [J]. Defence Technology, 2014, 10: 40−46.
[14] ROY S, SUWAS S. The influence of temperature and strain rate on the deformation response and microstructural evolution during hot compression of a titanium alloy Ti−6Al−4V−0.1B [J]. Journal of Alloys and Compounds, 2013, 548: 110−125.
[15] ABBASI S M, MOMENI A, LIN Y C, JAFARIAN H R. Dynamic softening mechanism in Ti−13V−11Cr−3Al beta Ti alloy during hot compressive deformation [J]. Materials Science and Engineering A, 2016, 665: 154−160.
[16] WU C, YANG H, FAN X, SUN Z. Dynamic globularization kinetics during hot working of TA15 titanium alloy with colony microstructure [J]. Transactions of Nonferrous Metals Society of China, 2011, 21: 1963−1969.
[17] WANG K, ZENG W, ZHAO Y, LAI Y, ZHOU Y. Dynamic globularization kinetics during hot working of Ti-17 alloy with initial lamellar microstructure [J]. Materials Science and Engineering A, 2010, 527: 2559−2566.
[18] ZHU Y, WANG H, GAO Z, CAI W. Martensitic transformation and microstructure of dual-phase Ti44Ni47Nb9 shape memory alloy after high-velocity impact [J]. Materials Characterization, 2016, 122: 162−169.
[19] SOUZA P M, BELADI H, SINGH R, ROLFE B, HODGSON P D. Constitutive analysis of hot deformation behavior of a Ti6Al4V alloy using physical based model [J]. Materials Science and Engineering A, 2015, 648: 265−273.
[20] MUTOMBO K, SIYASIYA C, STUMPF W E. Dynamic globularization of α-phase in Ti6Al4V alloy during hot compression [J]. Materials Science Forum, 2014, 783−786: 584−590.
[21] MA X, ZENG W, TIAN F, ZHOU Y. The kinetics of dynamic globularization during hot working of a two phase titanium alloy with starting lamellar microstructure [J]. Materials Science and Engineering A, 2012, 548: 6−11.
[22] ANDERSSON J O, HELANDER T, HOGLUND L, SHI P, SUNDMAN B. Thermo-Calc & DICTRA, computational tools for materials science [J]. Calphad, 2002, 26: 273−312.
[23] DIETER G E. Mechanical metallurgy [M]. Third ed. Boston, USA: McGraw-Hill, 1986.
[24] SHAO G, TSAKIROPOULOS P, MIODOWNIK A P. Phase transformations in Ti−40Al−10V [J]. Intermetallics, 1995, 3: 315−325.
[25] CARREON H, RUIZ A, SANTOVEÑA B. Study of aging effects in a Ti−6AL−4V alloy with widmanstätten and equiaxed microstructures by non-destructive means [C]//Proc AIP Conference, 2014: 739−745.
[26] LEE D G, LEE S, LEE C S. Quasi-static and dynamic deformation behavior of Ti−6Al−4V alloy containing fine α_2-Ti_3Al precipitates [J]. Materials Science and Engineering A, 2004, 366: 25−37.
[27] PRABHA JOSEPHINE A, RAJU S, JEYAGANESH B, RAI A K, BEHERA M, VIJAYALAKSHMI M, PANEERSELVAM G, JOHNSON I. Thermodynamics of $\alpha''\rightarrow\beta$ phase transformation and heat capacity measurements in Ti−15at%Nb alloy [J]. Physica B: Condensed Matter, 2011, 406: 4200−4209.
[28] SEMIATIN S, SEETHARAMAN V, WEISS I. Flow behavior and globularization kinetics during hot working of Ti−6Al−4V with a colony alpha microstructure [J]. Materials Science and Engineering A, 1999, 263: 257−271.
[29] BIELER T R, SEMIATIN S. The origins of heterogeneous deformation during primary hot working of Ti−6Al−4V [J]. International Journal of Plasticity, 2002, 18: 1165−1189.
[30] HE L, MANSHADI D A, DIPPENAAR R J. The evolution of microstructure of Ti−6Al−4V alloy during concurrent hot deformation and phase transformation [J]. Materials Science and Engineering A, 2012, 549: 163−167.

Ti6Al4V 合金等温压缩时的扩散相变

K. MUTOMBO[1], C. SIYASIYA[2], W. E. STUMPF[2]

1. Council for Scientific and Industrial Research (CSIR), Pretoria 0001, South Africa;
2. Department of Materials Science and Metallurgical Engineering, University of Pretoria, Pretoria 0001, South Africa

摘　要：利用 CompuTherm Pandat™软件及其自带的 Ti 数据库完成对双相 Ti 合金的热力学计算。对 Ti6Al4V (5 级)合金进行等温压缩，合金的初始组织为由层片状的(α+β)和 β 相组成的层片团结构。采用 X 射线衍射分析、扫描电镜和透射电镜表征材料的显微组织演化和相转变。用吉布斯自由能−温度和相含量−温度关系图预 Ti_3Al 或 α_2 (hcp)相的存在、稳定性和相变温度。等温压缩后，(α+β)相区的特征为 α/β 片层的重新定向和局部扭曲以及在 α/β 界面区的开裂。而在 $\alpha\rightarrow\beta$ 相变区，β 相和 α/β 相界发生变形，大量的 α 相转变为 β 相，板条状 α 相发生马氏体相变和球化。在 β 相区，α 相完全转变为 β 单相。结果表明，变形 Ti6Al4V 合金中形成 Ti_3Al 或 α_2(hcp)、β(bcc)和 α(hcp)相以及密排六方 α'和斜方 α''相。变形温度对屈服应力水平、动态回复和动态球化均存在影响。

关键词：Ti6Al4V；相变；球化；热力学计算

(Edited by Bing YANG)